


RESEARCH

Open Access



Evaluation of accuracy and membrane perforation in robotic-assisted implant surgery for transalveolar sinus floor elevation: a retrospective case series

Tao Yang^{1,2}, Wenjing Yi^{1,2}, Wenan Xu^{1,2}, Xiaojian Xing^{1,2} and Buling Wu^{1,2*} 

Abstract

Background The potential of the robotic system for transalveolar sinus floor elevation (TSFE) with simultaneous implant placement has not been verified. This study aimed to assess implant placement accuracy and membrane perforation in robotic computer-assisted implant surgery (r-CAIS) for TSFE.

Methods Patients who underwent r-CAIS for TSFE were enrolled in this study. Positioning markers were placed in the patient's oral cavity, and cone-beam computed tomography (CBCT) was performed. Subsequently, the surgical plan was generated using robotic software. After the markers were registered with the robotic arm, TSFE and implant placement were performed using the robotic arm and crestal approach sinus (CAS) kit drills under the control of the surgeons. Deviations between the planned and placed implants were assessed using preoperative and post-operative CBCT data. In addition, perforation of the Schneiderian membrane was evaluated intraoperatively using the Valsalva maneuver and postoperatively using CBCT images.

Results Ten patients were enrolled, and no adverse events occurred during the surgery. The mean global coronal, global apical, and angular deviations were 0.55 ± 0.20 mm (95% confidence interval [CI]: 0.41 to 0.69 mm), 0.56 ± 0.23 mm (95%CI: 0.40 to 0.73 mm), and $1.38 \pm 0.83^\circ$ (95%CI: 0.78 to 1.97°), respectively. No membrane perforation was observed during or after the surgery.

Conclusions Within the limitations of this study, r-CAIS for TSFE showed high accuracy and a low membrane perforation rate.

Keywords Implant placement, Transalveolar sinus floor elevation, Computer-assisted implant surgery, Crestal approach sinus kit, Robotic surgery

Background

The accuracy of dental implantation is closely linked to the aesthetic outcomes and long-term stability of the bone and soft tissues [1–3]. Conventional freehand implantation relies heavily on the surgeon's expertise; therefore, there is considerable susceptibility to surgical errors, particularly during complex procedures. The integration of computer-assisted technologies has effectively mitigated these errors.

*Correspondence:

Buling Wu
bulingwu@smu.edu.cn

¹ Shenzhen Clinical College of Stomatology, School of Stomatology, Southern Medical University, Shenzhen, Guangdong, China

² Shenzhen Stomatology Hospital (Pingshan) of Southern Medical University, No. 143, Dongzong Road, Pingshan District, Shenzhen, Guangdong 518118, China



© The Author(s) 2025. **Open Access** This article is licensed under a Creative Commons Attribution-NonCommercial-NoDerivatives 4.0 International License, which permits any non-commercial use, sharing, distribution and reproduction in any medium or format, as long as you give appropriate credit to the original author(s) and the source, provide a link to the Creative Commons licence, and indicate if you modified the licensed material. You do not have permission under this licence to share adapted material derived from this article or parts of it. The images or other third party material in this article are included in the article's Creative Commons licence, unless indicated otherwise in a credit line to the material. If material is not included in the article's Creative Commons licence and your intended use is not permitted by statutory regulation or exceeds the permitted use, you will need to obtain permission directly from the copyright holder. To view a copy of this licence, visit <http://creativecommons.org/licenses/by-nc-nd/4.0/>.

At present, three primary types of computer-assisted technologies are utilized in dental implant surgeries: static computer-assisted implant surgery (s-CAIS), dynamic computer-assisted implant surgery (d-CAIS), and robotic computer-assisted implant surgery (r-CAIS). An *in vitro* study indicated that the accuracy of d-CAIS was comparable to that of s-CAIS and surpassed that of freehand implantation [4]. Despite their success, both s-CAIS and d-CAIS have inherent limitations. The use of surgical guides in s-CAIS affects cooling and increases the risk of thermal injury to the bone [5]. Furthermore, because of their prefabricated nature, modifications to the surgical plan during surgery are not feasible [1, 6]. d-CAIS also demands a specific learning curve and necessitates continuous adjustment of the surgeon's vision between the surgical area and the computer screen during surgery [7, 8]. Furthermore, compared with that used in freehand implantation, the handpiece used in d-CAIS has a greater weight and volume, and this further increases the surgeon's fatigue during the procedure [1].

The advent of r-CAIS has ushered in transformative advancements in computer-assisted technologies [3, 9]. *In vitro* studies have indicated that the precision of r-CAIS surpasses that of both s-CAIS and d-CAIS [1, 10]. In addition, in a meta-analysis of 67 studies, r-CAIS exhibited lower deviations than did s-CAIS and d-CAIS. The results showed that s-CAIS, d-CAIS and r-CAIS exhibited a mean coronal deviation of 1.11 mm, 1.18 mm, and 0.81 mm, respectively; a mean apical deviation of 1.44 mm, 1.36 mm, and 0.77 mm, respectively; and a mean angular deviation of 3.58°, 3.51°, and 1.71°, respectively [11]. In other studies, r-CAIS achieved high accuracy in single-tooth [12], immediate [13], and fully edentulous implant placement [14]. However, evidence of its usefulness for maxillary sinus elevation remains limited.

Surgery for implant placement in the posterior maxilla is inherently complex because of the proximity to the maxillary sinus. The presence of the maxillary sinus results in inadequate bone availability, necessitating additional bone augmentation surgery to complete the implantation procedure [15]. Sinus lift surgery has emerged as the preferred approach to address this challenge [16]. This surgical intervention typically involves lateral window sinus floor elevation and transalveolar sinus floor elevation (TSFE) [17], with the latter being particularly recommended for mild to moderate alveolar ridge atrophy [18, 19].

However, because TSFE is a highly technical procedure, prevention of postoperative complications can be challenging. TSFE was initially introduced by Summers [20], who used a specialized osteotome to elevate the sinus floor along with the Schneiderian membrane.

Nevertheless, the application of Summers TSFE is limited because of the discomfort experienced by patients during the percussive process, as well as postoperative complications such as headache, swelling, and benign paroxysmal vertigo, which has an incidence of 5.84% [21, 22]. Membrane perforation is another notable concern; a systematic review reported a membrane perforation rate of 0 to 21% [23].

Various nonpercussive sinus lift techniques have been utilized to improve the management of intraoperative discomfort during Summers TSFE and minimize the associated complications [19, 24, 25]. The crestal approach sinus (CAS) kit, which uses a specialized intermittent, non-cutting drill that preserves the integrity of the Schneiderian membrane while penetrating the sinus floor, has indicated safety and efficacy when used for TSFE [26, 27]. However, the surgeon's proficiency significantly influences the success of this approach because the drills must be retracted when encountering a sudden decrease in bone resistance. In an *ex vivo* study, the incidence of membrane perforation was 8.3% [28]. Therefore, more precise instruments are required to replace subjective assessments based on the surgeon's experience.

In a recent model study, r-CAIS was equipped with a real-time force feedback function that provided surgeons with a reliable point of reference during TSFE [27]. Another clinical case report demonstrated the feasibility of r-CAIS for TSFE [29]. However, further clinical studies are required to confirm the efficacy of this technique. Thus, the aim of the present study was to integrate r-CAIS with CAS kit drills to facilitate a safer TSFE procedure with enhanced implant placement accuracy.

Methods

Study design and population

This was a retrospective case series evaluating the utility of r-CAIS for TSFE with simultaneous implant placement. The study protocol was approved by the local Ethics Committee (No. 202412A) and followed the guidelines of the Declaration of Helsinki. Patients were identified from specialized records in the Department of Implant Dentistry between Dec 2023 and May 2024. All patients received a comprehensive explanation of potential intraoperative and postoperative complications and subsequently provided written informed consent.

The inclusion criteria were as follows: (1) TSFE with r-CAIS and CAS kit drills (OSSTEM, Seoul, South Korea, Fig. 1A), (2) absence of significant inflammation or cyst formation in the maxillary sinus, (3) age ≥ 18 years, (4) no smoking or light smoking (< 10 cigarettes/day), (5) satisfactory treatment compliance, and (6) good general health and oral hygiene. The exclusion criteria were as follows: (1) uncontrolled systemic or periodontal disease,

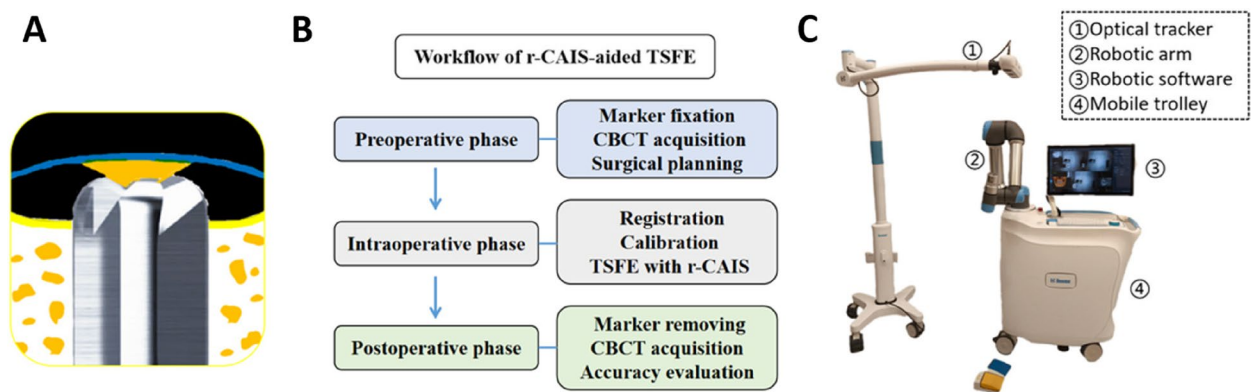


Fig. 1 Workflow during r-CAIS for TSFE. **A** CAS kit drill. **B** r-CAIS workflow. **C** Robotic system

(2) general contraindications for implant placement, (3) pregnancy or lactation, (4) heavy smoking (>10 cigarettes/day) or alcoholism, (5) allergic rhinitis and chronic recurrent sinusitis, (6) local aggressive benign or malignant tumors, and (7) insufficient medical compliance.

r-CAIS workflow

The r-CAIS workflow was divided into preoperative, operative, and postoperative phases, as illustrated in Fig. 1B.

Preoperative phase

The robotic system (Remebot, Baihui Weikang, Beijing, China, Fig. 1C) was preheated and debugged to ensure regular operation of the hardware and software. Patients were administered antibiotics 30 min before the surgery and instructed to rinse their mouths with a 0.12% chlorhexidine solution three times for 1 min each. A universal positioning marker with seven ceramic balls (Baihui Weikang, Beijing, China) was selected based on the surgical region. Subsequently, the teeth on the contralateral side were selected and dried, and self-curing acrylic resin (Protemp™, 3 M ESPE, Neuss, Germany) was injected

into the marker and placed in the patients' teeth until it solidified. Subsequently, the patients were directed to bite down on a piece of gauze to prevent contact with the marker, and CBCT (KAVO, Biberach, Germany) was performed with parameters set at 120 kV/1.38 mA, a 0.25-mm voxel size, and a scanning time of 26.9 s. Digital Imaging and Communications in Medicine (DICOM) format data were then transferred to the robotic software for preoperative planning. After the surgeon and engineer confirmed the details, a specialized surgical plan was generated. For improved visualization of the real-time positional relationship between the drills and the maxillary sinus floor, the latter was demarcated with a yellow line in the software (Fig. 2).

Operative phase

After intraoral and extraoral disinfection three times, local infiltration anesthesia was administered using Primacaine® (4% Articaine, 1:100,000 adrenaline, ACTEON, M'érignac, France). Following the onset of anesthesia, a linear incision was made in the mucosa of the surgical area after positioning of the marker (Fig. 3A), and the robotic arm was registered. The mucoperiosteal flap was

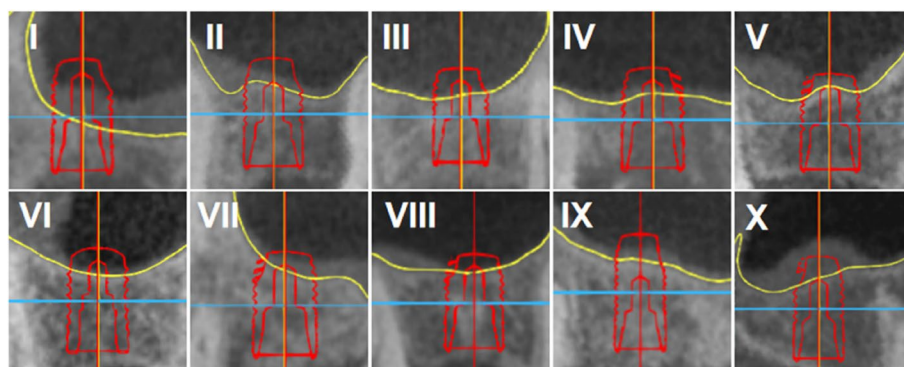


Fig. 2 Preoperative surgical design of coronal plane for each case. The sinus floor is marked with a yellow line



Fig. 3 TSFE using r-CAIS. **A** A universal positioning marker. **B** The surgery is guided by a robotic arm. **C** Real-time computer screen showing the robotic surgery

elevated, and any remaining granulation tissue on the bone surface was removed. Subsequently, the surgeon maneuvered the robotic arm near the surgical area and directed it to perform the procedure (Fig. 3B). The available bone volume and depth were assessed in the software, according to the presurgical design, at 1.5–2.0 mm from the sinus floor. Then, the relevant serial drills of the implant system were used to reach the drilling depth. Subsequently, a CAS kit drill with an appropriate diameter was selected, and the r-CAIS system was switched to the TSFE mode (Fig. 3C). The robotic arm automatically retracted when a sudden decrease in resistance

was indicated by the system, with real-time monitoring of force value changes during the lifting process (Fig. 4). Sinus floor bone penetration was manually verified using a depth gauge. Concurrently, Schneiderian membrane perforation was assessed using the Valsalva maneuver. A bone substitute material (Bio-oss, Geistlich, Wolhusen, Switzerland) was gradually introduced into the cavity several times and gently pressurized to elevate the Schneiderian membrane. After repeated Valsalva maneuvers, the implant was placed by the robotic arm. If the insertion torque exceeded 15 N.cm, a healing cap was installed. Conversely, if the value was less than 15 N.cm, a

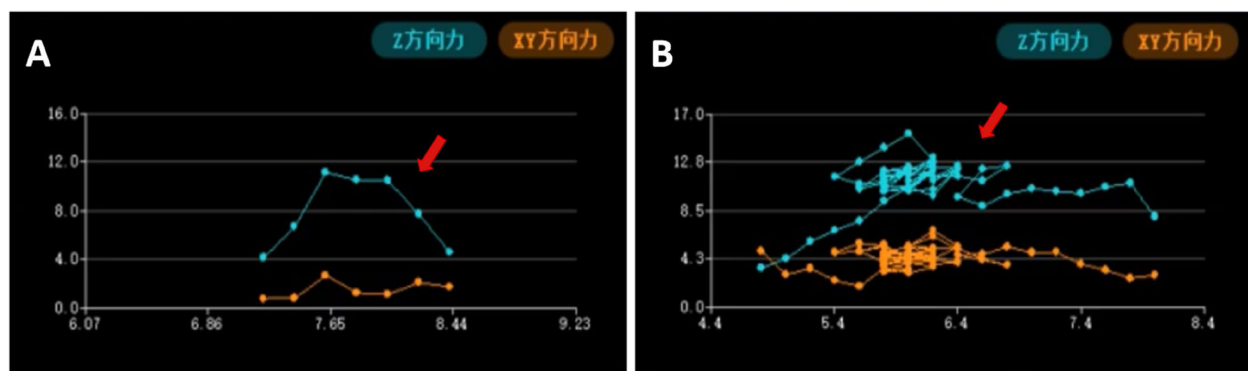


Fig. 4 Real-time force feedback system interface for TSFE using r-CAIS. **A** Low bone density near the sinus floor. **B** High bone density near the sinus floor

cover screw was installed. The wounds were sutured with nonabsorbable polypropylene sutures (Ethicon, Johnson & Johnson, New Jersey, United States).

Postoperative phase

The patients received instructions for postoperative care and were asked to refrain from flying or diving for 2 weeks. They were also instructed to avoid blowing their noses with excessive force and to rinse their oral cavities with a 0.12% chlorhexidine solution twice daily for 7 days. Furthermore, they were prescribed oral systemic antibiotics (0.25 g cefaclor, three times daily for 7 days) and analgesics (0.5 g acetaminophen tablets, three times daily as needed). The sutures were removed 2 weeks after surgery.

Accuracy analysis

After the surgery, the patients underwent postoperative CBCT scanning. The DICOM data acquired before and after surgery were incorporated and assessed using robotic software (RemebotDent, Baihui Weikang, Beijing, China). Subsequently, utilizing the central axis of both the planned and placed implants (Fig. 5) as reference, the robotic software generated an accuracy report, including coronal (global, lateral, and vertical) and apical (global, lateral, and vertical) deviations in millimeters as well as the angular deviation in degrees.

Evaluation of Schneiderian membrane perforation

After the surgical procedure, Schneiderian membrane perforation was assessed using the Valsalva maneuver. Postoperative CBCT was subsequently performed to assess Schneiderian membrane integrity. Evaluations were conducted by two oral and maxillofacial radiologists, each with over five years of specialized experience in CBCT analysis for TSFE. The reviewers were blinded to surgical protocols and patient outcomes, and assessments were conducted according to the following criteria: (1) observation of a tent-like elevation of the membrane surrounding the apex of the implant and (2) the absence of any obstructions beyond the Schneiderian membrane in the maxillary sinus on X-ray images, such as low-density sanguineous fluids or high-density particles of the bone substitute material.

Statistical analysis

Quantitative data are expressed as standard descriptive statistics, encompassing means, standard deviations, maximum and minimum values, and upper and lower 95% confidence intervals (CIs). All statistical analyses were conducted using SPSS software (version 23.0; IBM Corp., New York, United States).

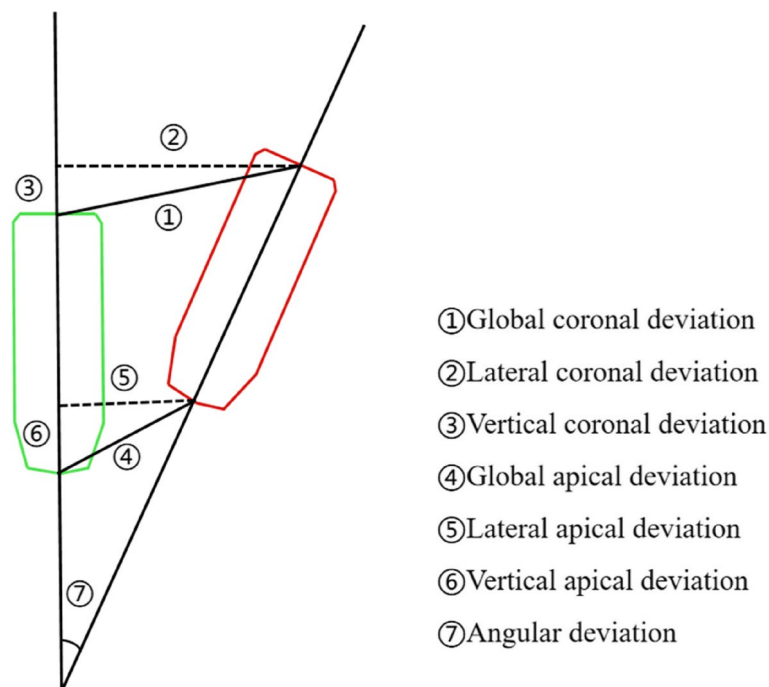


Fig. 5 Graphical representation of deviations between the planned and placed implants

Results

Patient characteristics

In total, ten patients, including five male and five female patients aged 26–60 (mean: 42.8 ± 11.9) years, were enrolled. All patients underwent TSFE surgery with concurrent implant placement, and none experienced surgical complications or postoperative events. Table 1 provides an overview of the demographic and surgical characteristics of the patients. One premolar and

nine molars required replacement with implants in this study. Cylindrical implants with diameters ranging from 4.2 to 4.8 mm and lengths ranging from 8 to 11 mm were used. The insertion torque varied from 5 to 35 N.cm.

Accuracy

Figure 6 depicts the pre- and postoperative fusion images, and Table 2 presents the quantitative outcomes. The

Table 1 Demographic and surgical characteristics of patients

Patient No	Age	Sex	Site	Implant type	Implant geometry	Implant size	Insertion Torque (N.cm)
I	39	M	15	Astra EV	cylindrical	4.2×8	5
II	60	F	16	Astra EV	cylindrical	4.8×9	10
III	39	M	16	Astra EV	cylindrical	4.8×8	10
IV	35	M	17	Astra EV	cylindrical	4.8×8	5
V	33	M	26	Astra EV	cylindrical	4.8×8	10
VI	36	F	26	Straumann BL	cylindrical	4.8×8	35
VII	44	M	26	Astra EV	cylindrical	4.8×8	35
VIII	26	M	26	Astra EV	cylindrical	4.8×8	15
IX	57	F	26	Astra EV	cylindrical	4.8×11	35
X	59	F	26	Astra EV	cylindrical	4.2×9	10

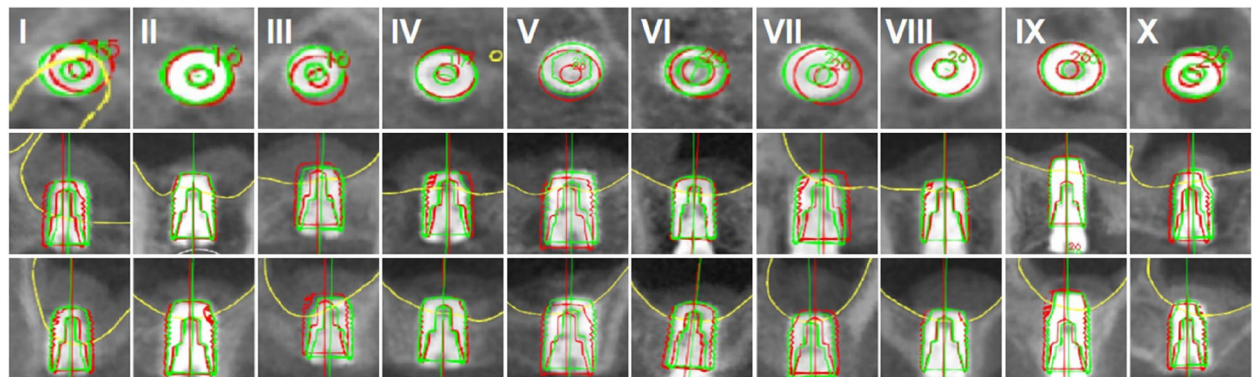


Fig. 6 CBCT fusion images of the planned and placed implants for each case. The transverse, coronal, and sagittal planes are indicated by the first, second, and third lines, respectively. Planned implants are outlined in red, and the placed implants are outlined in green

Table 2 Descriptive statistics for implant deviations

Deviation	Mean	Standard deviation	Max	Min	Median	Lower 95% CIs	Upper 95% CIs
Global coronal deviation (mm)	0.55	0.20	0.78	0.18	0.57	0.41	0.69
Lateral coronal deviation (mm)	0.44	0.12	0.57	0.18	0.46	0.35	0.53
Vertical coronal deviation (mm)	0.02	0.37	0.62	−0.55	0.06	−0.25	0.28
Global apical deviation (mm)	0.56	0.23	0.95	0.27	0.56	0.40	0.73
Lateral apical deviation (mm)	0.46	0.16	0.76	0.27	0.42	0.35	0.58
Vertical apical deviation (mm)	0.02	0.37	0.62	−0.56	0.06	−0.25	0.28
Angular deviation (°)	1.38	0.83	3.2	0.45	1.22	0.78	1.97

mean global, lateral, and vertical coronal deviations were 0.55 ± 0.20 mm (95%CI:0.41 to 0.69 mm), 0.44 ± 0.12 mm (95%CI:0.35 to 0.53 mm) and 0.02 ± 0.37 mm (95%CI:-0.25 to 0.28 mm), respectively. The mean global, lateral, and vertical apical deviations were 0.56 ± 0.23 mm (95%CI:0.40 to 0.73 mm), 0.46 ± 0.16 mm (95%CI:0.35 to 0.58 mm), and 0.02 ± 0.37 mm (95%CI:-0.25 to 0.28 mm), respectively. The mean angular deviation was $1.38 \pm 0.83^\circ$ (0.78 to 1.97°). Figures 7 and 8 show the global coronal, global apical, and angular deviations for each case.

Schneiderian membrane evaluation

Schneiderian membrane perforation was not identified during the intraoperative Valsalva maneuver or subsequent postoperative assessment using CBCT in any case, as illustrated in Fig. 9.

Discussion

This study indicated the potential of r-CAIS as a viable technology for TSFE with simultaneous implant placement. The mean global coronal, apical, and angular

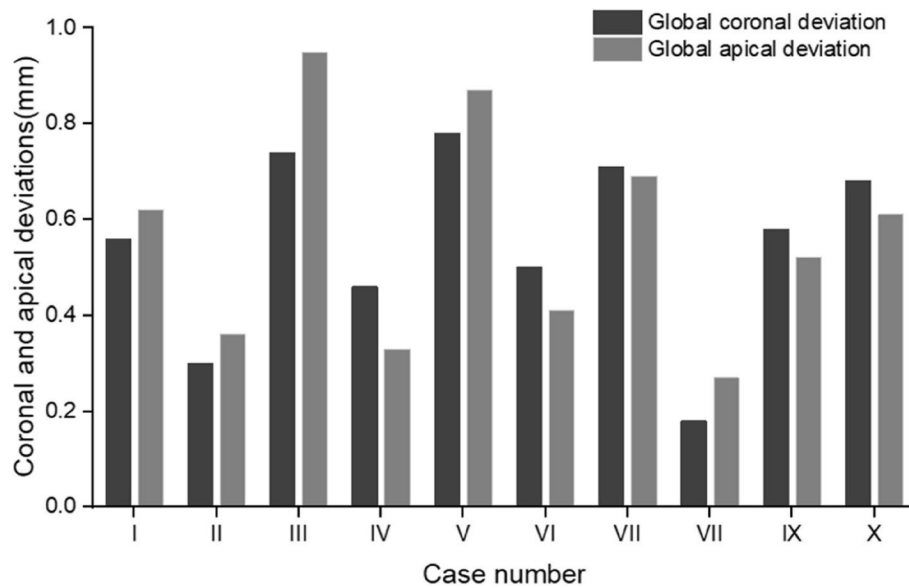


Fig. 7 Global coronal and apical deviations in each case

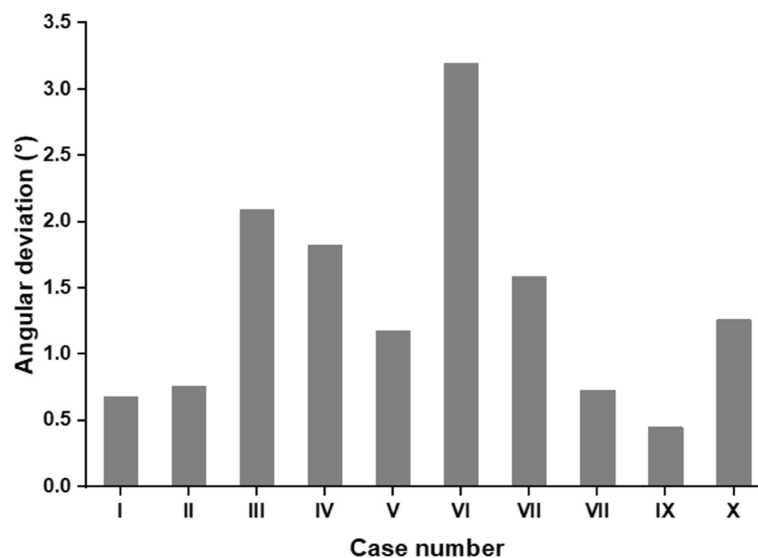


Fig. 8 Angular deviation in each case

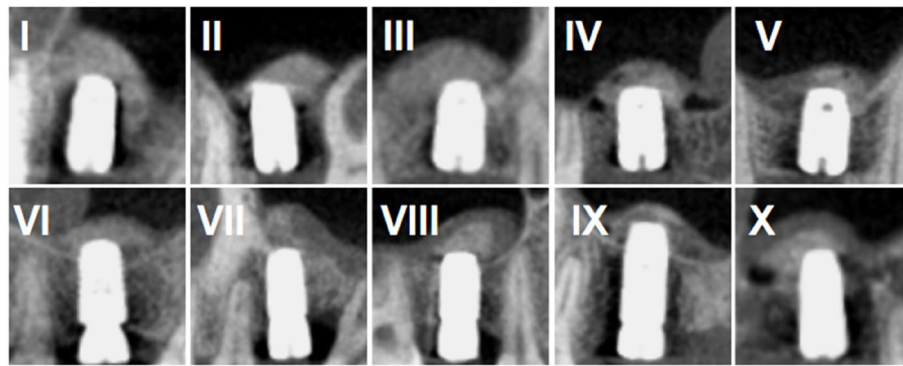


Fig. 9 Postoperative CBCT image of each case

deviations were 0.55 ± 0.20 mm, 0.56 ± 0.23 mm, and $1.38 \pm 0.83^\circ$, respectively. Notably, no membrane perforation was observed. To the best of our knowledge, this is the first case series to investigate the application of r-CAIS for TSFE with simultaneous implant placement, thereby expanding the current literature on this emerging technique.

s-CAIS and d-CAIS have indicated high accuracy in implant placement surgery. A multicenter, retrospective clinical study involving 61 implants revealed that the mean coronal, apical, and angular deviations with s-CAIS were 0.73 mm, 1.06 mm, and 2.94° , respectively [6]. Furthermore, a meta-analysis of 24 clinical studies indicated that the entry and angular deviations with d-CAIS were 1.03 mm and 3.68° , respectively [30]. However, it should be noted that the observed deviations significantly exceeded those observed in the present study; this indicated that the accuracy of r-CAIS surpasses that of s-CAIS and d-CAIS.

The maxillary posterior regions generally present with low bone density and reduced bone volume. Although short implants have been reported to be successfully applied in atrophic posterior jaws [31, 32], TSFE remains the most commonly employed procedure, utilizing longer implants to achieve enhanced biomechanical stability. In such cases, precise implant placement is crucial to minimize stress on the implants after restoration. Computer-assisted surgery, such as s-CAIS, can help minimize deviations. A randomized controlled clinical trial revealed that fully guided s-CAIS for TSFE resulted in platform, apical, and angular deviations of 1.37 mm, 1.85 mm, and 4.69° , respectively, whereas partially guided s-CAIS for TSFE yielded even higher deviations of 2.02 mm, 2.57 mm, and 6.65° , respectively [33]. These deviations were significantly greater than those observed in our study, possibly because of introduction of the robotic arm. According to the manufacturer's data, the repeatability accuracy of the robotic arm is 0.033 mm,

enabling precise implementation of the surgical plan. In addition, the robotic arm demonstrates exceptional stability during surgery, whereas s-CAIS requires surgeons to manually hold the guides, leading to inevitable deviations resulting from inherent errors associated with the gap between the metal sleeves and drills [10].

Given the lack of research related to the utilization of r-CAIS for TSFE, we performed a comparative analysis with extant studies on r-CAIS used in other facets of dental implantation. A case series on single-tooth implant placement using r-CAIS revealed mean coronal, apical, and angular deviations of 0.74 ± 0.29 mm, 0.73 ± 0.28 mm, and $1.11 \pm 0.46^\circ$, respectively [12]. A retrospective study involving fully edentulous patients demonstrated mean coronal, apical, and angular deviations of 0.67 ± 0.37 mm, 0.69 ± 0.37 mm, and $1.27 \pm 0.59^\circ$, respectively [14]. These studies were as sound and consistent as the present study; however, the angular deviation ($1.38 \pm 0.83^\circ$) observed in the present study was marginally higher than that reported in the aforementioned studies, possibly because the implants in the present study had their apices partially submerged in the maxillary sinus, which could potentially lead to increased axial deviations during the surgical procedure.

Membrane perforation is the most prevalent complication of TSFE [34]. This study employed the Valsalva maneuver during surgery and postoperative evaluation using CBCT to determine the presence of Schneiderian membrane perforation, as recommended in previous studies [35–37]. Our verification using both methods indicated that r-CAIS for TSFE effectively protects the Schneiderian membrane, given the absence of membrane perforation in this study.

The diverse morphology of the maxillary sinus floor plays a pivotal role in the incidence of membrane perforation during TSFE. Specifically, a steep sinus floor morphology is associated with a higher risk of membrane perforation than is a flat morphology [27]. In the present

study, cases involving a steep sinus floor morphology (Cases I, II, V, and VII) did not exhibit membrane perforation, possibly because of the incorporation of a real-time force feedback system within the r-CAIS device. This real-time force feedback system played a crucial role in ensuring high accuracy and minimizing membrane perforation during the TSFE procedure. Throughout the procedure, the real-time position and axial orientation of the implant were presented on a computer screen that typically features depth cues along with live displays of the transverse, coronal, and sagittal positions. This enables surgeons to intuitively recognize subtle errors that may arise during implantation, allowing for timely adjustments [3].

In addition, in contrast to previous nonpercussive TSFE techniques (compared with the Summers method) [19, 24, 25, 36], our approach for penetration of the sinus floor did not rely on the subjective perception of the surgeons. Instead, it was guided by the mechanical feedback system of r-CAIS. Throughout the procedure, the resistance of the bone to the drills was transmitted to the robotic arm. As shown in Fig. 4, the resultant force acting on the drill comprises components along the X, Y, and Z axes. When a sudden decrease in the resultant force is detected, the robotic system promptly receives feedback and rapidly retracts its arm. According to the manufacturer, the response time can be as fast as 0.06 s.

During the drilling process, the robotic arm adjusts the drilling depth based on the applied force. The manufacturer incorporates three features into the r-CAIS TSFE system. First, when the resultant force falls below 8 N.cm, the system advances the drill by 0.2 mm (Fig. 4A, indicated by the red arrow). Second, when the resultant force ranges between 8 and 12 N.cm, in situ cutting occurs until the resultant force decreases below 8 N.cm (Fig. 4B, indicated by the red arrow). Third, if the resultant force exceeds 12 N.cm, the system retracts the drill by 0.2 mm to minimize stress on the bone. This 0.2-mm increase in the drilling depth closely resembles the drilling procedure with the manual CAS kit, which has serial depth-restricting metal sleeves leading to depth restriction in increments of 1 mm per surgery [26]. However, introduction of the robotic arm has significantly enhanced the operative sensitivity from 1 mm to 0.2 mm.

Moreover, during the drilling overshoot process, the force feedback system of r-CAIS consistently controls the peak force value. If this force undergoes an abrupt 70% decrease and demonstrates a downward trajectory across four consecutive calculation cycles, the de-drilling mechanism is engaged, leading to immediate withdrawal of the robotic arm. This process can also be programmed to effectuate a complete fracture and withdrawal if the drills

detect a pressure drop below 4 N.cm for two consecutive calculation cycles.

In this study, the incidence of lower membrane perforation was associated with the use of CAS kit drills. These drills are characterized by a drill tip with a counter tapered configuration, which promotes the formation of a conical bone fragment during the drilling process. This design facilitates successful membrane elevation and has been previously reported to achieve favorable clinical outcomes in cases with severe alveolar bone resorption [26, 38]. Moreover, the bone particles generated during drilling are expelled in an upward direction, thereby facilitating automatic lifting of the membrane [27].

Notably, in this study, no intra- or postoperative adverse events or complications were reported. The conventional Summers technique employs a bone hammer and specialized instruments to penetrate the sinus floor. This percussive action can increase patient discomfort and anxiety during the procedure, potentially leading to benign paroxysmal vertigo and other related complications [21]. Although the improved nonpercussive free-hand surgical method mitigates these issues, it relies on the surgeon's subjective experience, which may increase the risk of surgical errors [28]. In this study, we applied r-CAIS combined with CAS kit drills to effectively address the challenges associated with conventional techniques used for TSFE. This innovative technology shows promise for future applications.

The use of r-CAIS for TSFE resulted in significant accuracy and a low incidence of membrane perforation. However, this study has several limitations. First, the preoperative procedures for r-CAIS are intricate and involve presurgical CBCT scanning, marker installation, preoperative design, and registration and calibration. These procedures prolong the surgical duration and may increase patient discomfort. Thus, there is a need to streamline the processes and enhance patient comfort. Second, the robotic entrance trajectory is relatively fixed, leading to limited access to the maxillary posterior tooth regions, thus increasing the complexity of the surgery. In case IV, we alternated between the manual and automatic modes during the TSFE procedure for the maxillary second molar. Further investigations should focus on optimizing the effectiveness of robotic surgeries in cases with limited mouth opening. Third, the sample size was small without a control group, and the residual bone volume and sinus floor morphology were not categorized, underscoring the need for larger-scale, multicenter, randomized controlled trials to validate the clinical efficacy. Finally, this study primarily focused on the accuracy of r-CAIS and Schneiderian membrane perforation, neglecting patient satisfaction and long-term clinical

outcomes. Future studies should include these parameters to provide a more comprehensive assessment.

Conclusions

Within the context of the study limitations, the findings indicate that the use of r-CAIS for TSFE with simultaneous implant placement can substantially improve the implant placement accuracy and preserve membrane integrity. However, further prospective clinical studies are required to substantiate and validate these observed outcomes.

Abbreviations

TSFE	Transalveolar sinus floor elevation
CAS	Crestal approach sinus
CBCT	Cone-beam computed tomography
s-CAIS	Static computer-assisted implant surgery
d-CAIS	Dynamic computer-assisted implant surgery
r-CAIS	Robotic computer-assisted implant surgery
DICOM	Digital Imaging and Communications in Medicine

Acknowledgements

The authors would like to acknowledge the excellent technical assistance of Dingjun Zhong from Beijing RuiYiBo Technology Co., Ltd.

Authors' contributions

Tao Yang: Writing – review & editing, Writing – original draft, Funding acquisition, Data curation, Conceptualization, Software. Wenjing Yi: Writing – review & editing, Writing – original draft, Data curation, Software. Wenan Xu: Writing – review & editing, Software, Conceptualization. Xiaojian Xing: Writing – review & editing, Validation, Supervision. Buling Wu: Writing – review & editing, Supervision, Data curation, Funding acquisition, Project administration, Resources.

Funding

This study was supported by grants from Shenzhen Science and Technology Program (No: JCYJ20220530162408020) and the President Foundation of Shenzhen Stomatology Hospital (Pingshan), Southern Medical University (No:2022A001 and 2022C003).

Data availability

The data that support the findings of this study are available from the corresponding author upon reasonable request.

Declarations

Ethics approval and consent to participate

The study was approved by the Ethics Committee of Shenzhen Stomatology Hospital (Pingshan) of Southern Medical University (Number: 202412A) and followed the guidelines of the Declaration of Helsinki. All patients provided written informed consent.

Consent for publication

No applicable.

Competing interests

The authors declare no competing interests.

Received: 7 January 2025 Accepted: 19 March 2025

Published online: 03 April 2025

References

- Chen J, Bai X, Ding Y, Shen L, Sun X, Cao R, Yang F, Wang L. Comparison the accuracy of a novel implant robot surgery and dynamic navigation system in dental implant surgery: an in vitro pilot study. *BMC Oral Health*. 2023;23(1):179.
- Pomares-Puig C, Sánchez-Garcés MA, Jorba-García A. Dynamic and static computer-assisted implant surgery for completely edentulous patients. A proof of a concept. *J Dent*. 2023;130:104443.
- Yang T, Xu W, Xing X, Li F, Yang S, Wu B. Accuracy of robotic-assisted surgery for immediate implant placement in posterior teeth: a retrospective case series. *BMC Oral Health*. 2024;24(1):1263.
- Kivovics M, Takács A, Péntes D, Németh O, Mijiritsky E. Accuracy of dental implant placement using augmented reality-based navigation, static computer assisted implant surgery, and the free-hand method: An in vitro study. *J Dent*. 2022;119:104070.
- Geng N, Ren J, Zhang C, Zhou T, Feng C, Chen S. Immediate implant placement in the posterior mandibular region was assisted by dynamic real-time navigation: a retrospective study. *BMC Oral Health*. 2024;24(1):208.
- Luongo F, Lerner H, Gesso C, Sormani A, Kalemaj Z, Luongo G. Accuracy in static guided implant surgery: Results from a multicenter retrospective clinical study on 21 patients treated in three private practices. *J Dent*. 2024;140:104795.
- Panchal N, Mahmood L, Retana A, Emery R 3rd. Dynamic Navigation for Dental Implant Surgery. *Oral Maxillofac Surg Clin North Am*. 2019;31(4):539–47.
- Wang XY, Liu L, Guan MS, Liu Q, Zhao T, Li HB. The accuracy and learning curve of active and passive dynamic navigation-guided dental implant surgery: An in vitro study. *J Dent*. 2022;124:104240.
- Wu Y, Wang F, Fan S, Chow JK. Robotics in Dental Implantology. *Oral Maxillofac Surg Clin North Am*. 2019;31(3):513–8.
- He J, Zhang Q, Wang X, Fu M, Zhang H, Song L, Pu R, Jiang Z, Yang G. In vitro and in vivo accuracy of autonomous robotic vs. fully guided static computer-assisted implant surgery. *Clin Implant Dent Relat Res*. 2024;26(2):385–401.
- Khaochoen A, Powcharoen W, Sornsuan T, Chaijareenont P, Rungsiyakul C, Rungsiyakul P. Accuracy of implant placement with computer-aided static, dynamic, and robot-assisted surgery: a systematic review and meta-analysis of clinical trials. *BMC Oral Health*. 2024;24(1):359.
- Yang S, Chen J, Li A, Deng K, Li P, Xu S. Accuracy of autonomous robotic surgery for single-tooth implant placement: A case series. *J Dent*. 2023;132:104451.
- Zhao N, Du L, Lv C, Liang J, He L, Zhou Q. Accuracy analysis of robotic-assisted immediate implant placement: A retrospective case series. *J Dent*. 2024;146:105035.
- Li P, Chen J, Li A, Luo K, Xu S, Yang S. Accuracy of autonomous robotic surgery for dental implant placement in fully edentulous patients: A retrospective case series study. *Clin Oral Implants Res*. 2023;34(12):1428–37.
- Testori T, Weinstein T, Taschieri S, Wallace SS. Risk factors in lateral window sinus elevation surgery. *Periodontol*. 2000. 2019;81(1):91–123.
- Al-Dajani M. Recent Trends in Sinus Lift Surgery and Their Clinical Implications. *Clin Implant Dent Relat Res*. 2016;18(1):204–12.
- Chen J, Lu Y, Xu J, Hua Z. Clinical evaluation of maxillary sinus floor elevation with or without bone grafts: a systematic review and meta-analysis of randomised controlled trials with trial sequential analysis. *Arch Med Sci*. 2024;20(2):384–401.
- Huang J, Ban C, Liu L, Ye Y. Dynamics and risk indicators of intrasinus elevation height following transalveolar sinus floor elevation with immediate implant placement: a longitudinal cohort study. *Int J Oral Maxillofac Surg*. 2021;50(1):109–15.
- Zhao X, Gao W, Liu F. Clinical evaluation of modified transalveolar sinus floor elevation and osteotome sinus floor elevation in posterior maxillae: study protocol for a randomized controlled trial. *Trials*. 2018;19(1):489.
- Summers RB. A new concept in maxillary implant surgery: the osteotome technique. *Compendium*. 1994;15(2):152, 154–6 158 passim; quiz 162.
- Di Girolamo M, Napolitano B, Arullani CA, Bruno E, Di Girolamo S. Paroxysmal positional vertigo as a complication of osteotome sinus floor elevation. *Eur Arch Otorhinolaryngol*. 2005;262(8):631–3.
- Esposito M, Cannizzaro G, Barausse C, Cosci F, Soardi E, Felice P. Cosci versus Summers technique for crestal sinus lift: 3-year results from a randomised controlled trial. *Eur J Oral Implantol*. 2014;7(2):129–37.
- Tan WC, Lang NP, Zwahlen M, Pjetursson BE. A systematic review of the success of sinus floor elevation and survival of implants inserted in combination with sinus floor elevation. Part II: transalveolar technique. *J Clin Periodontol*. 2008;35(8 Suppl):241–54.

24. Lozada JL, Goodacre C, Al-Ardah AJ, Garbacea A. Lateral and crestal bone planing antrostomy: a simplified surgical procedure to reduce the incidence of membrane perforation during maxillary sinus augmentation procedures. *J Prosthet Dent*. 2011;105(3):147–53.
25. Cho YS, Chong D, Yang SM, Kang B. Hydraulic Transcrestal Sinus Lift: Different Patterns of Elevation in Pig Sinuses. *Implant Dent*. 2017;26(5):706–10.
26. Wu H, Wang J, Wang C, Yang X, Gong Q, Su W, Cheng A, Fan Y. A Comparison of Elevation, Perforation Rate, and Time Spent for the Crestal Sinus Elevation Intervened by Piezosurgery, CAS-Kit, and Osteotome in a Novel Goat Model. *J Maxillofac Oral Surg*. 2022;21(4):1191–8.
27. Yu S, Wang Y, Wang Y, Miron RJ, Yan Q, Zhang Y. A transcrestal sinus floor elevation strategy based on a haptic robot system: An in vitro study. *Clin Implant Dent Relat Res*. 2024;26(6):1270–8.
28. Alsabbagh AY, Alsabbagh MM, Nahas BD, Rajih S. Correction to: Comparison of three different methods of internal sinus lifting for elevation heights of 7 mm: an ex vivo study. *Int J Implant Dent*. 2020;6(1):43.
29. Su X, Wang G, Zhao B, Wang X. Maxillary sinus floor elevation for implant placement assisted by an autonomous dental implant robotic system: A clinical report. *J Prosthet Dent*. 2024;S0022–3913(24):00241–5.
30. Jorba-García A, González-Barnadas A, Camps-Font O, Figueiredo R, Valmaseda-Castellón E. Accuracy assessment of dynamic computer-aided implant placement: a systematic review and meta-analysis. *Clin Oral Investig*. 2021;25(5):2479–94.
31. Esposito M, Barausse C, Pistilli R, Piattelli M, Di Simone S, Ippolito DR, Felice P. Posterior atrophic jaws rehabilitated with prostheses supported by 5 × 5 mm implants with a nanostructured calcium-incorporated titanium surface or by longer implants in augmented bone. Five-year results from a randomised controlled trial. *Int J Oral Implantol (Berl)*. 2019;12(1):39–54.
32. Esposito M, Barausse C, Pistilli R, Checchi V, Diazi M, Gatto MR, Felice P. Posterior jaws rehabilitated with partial prostheses supported by 4.0 × 4.0 mm or by longer implants: Four-month post-loading data from a randomised controlled trial. *Eur J Oral Implantol*. 2015;8(3):221–30.
33. Kim J, Park JY, Lee JY, Kim DM, Lee J, Jung UW, Lim YJ, Cha JK. Randomized controlled trial on the efficacy of a custom-made, fully guided implant system for flapless crestal sinus floor elevation: Accuracy and patient-reported outcomes. *Clin Oral Implants Res*. 2024;35(12):1531–45.
34. Soares LFF, Malzoni CMA, da Silveira ML, Junior EM, Pigossi SC. Evaluation of Different Approaches for Sinus Membrane Perforation Repair During Sinus Elevation: A Systematic Review and Meta-analysis. *Int J Oral Maxillofac Implants*. 2024;39(1):107–18.
35. Andrés-García R, Ríos-Santos JV, Herrero-Climent M, Bullón P, Fernández-Farhall J, Gómez-Menchero A, Fernández-Palacín A, Ríos-Carrasco B. Sinus Floor Elevation via an Osteotome Technique without Biomaterials. *Int J Environ Res Public Health*. 2021;18(3):1103.
36. Kim JM, Sohn DS, Bae MS, Moon JW, Lee JH, Park IS. Flapless transcrestal sinus augmentation using hydrodynamic piezoelectric internal sinus elevation with autologous concentrated growth factors alone. *Implant Dent*. 2014;23(2):168–74.
37. Pjetursson BE, Lang NP. Sinus floor elevation utilizing the transalveolar approach. *Periodontol 2000*. 2014;66(1):59–71.
38. Zadrozny Ł, Wagner L, Rosenbach D. Minimally Invasive Transcrestal Sinus Floor Elevation Procedure in Severely Atrophic Ridge: A Case Report. *J Oral Implantol*. 2021;47(3):215–22.

Publisher's Note

Springer Nature remains neutral with regard to jurisdictional claims in published maps and institutional affiliations.